Germline *RUNX1* Variation and Predisposition to Childhood Acute Lymphoblastic Leukemia

Yizhen Li, PhD[1], Meenakshi Devidas, PhD[2], Wentao Yang, PhD[1], Stuart S. Winter, MD[3], Wenjian Yang, PhD[1], Kimberly P. Dunsmore, MD[4], Colton Smith, PhD[1], Maoxiang Qian, PhD[5], Xujie Zhao, MS[1], Ranran Zhang, MS[1], Julie M. Gastier-Foster, PhD[6], Elizabeth A. Raetz, MD[7], William L. Carroll, MD[7], Chunliang Li, PhD[8], Paul P. Liu[9], Karen R. Rabin, MD, PhD[10], Takaomi Sanda[11,12], Charles G. Mullighan, MBBS, MD[13], Kim E. Nichols, MD[14], William E. Evans, PharmD[1,15], Ching-Hon Pui, MD[14,15], Stephen P. Hunger, MD[16], David T. Teachey[17], MD, Mary V. Relling, PharmD[1,14], Mignon L. Loh, MD[18], Jun J. Yang, PhD[1, 14, 15 f]

[1]Department of Pharmaceutical Sciences, St. Jude Children's Research Hospital, Memphis, TN, [2]Department of Global Pediatric Medicine, St. Jude Children's Research Hospital, Memphis, TN, [3]Children's Minnesota Research Institute, Children's Minnesota, Minneapolis, MN,[4]Children's Hematology and Oncology, Carilion Clinic and Virginia Tech Carilion School of Medicine, Roanoke, VA, [5]Children's Hospital and Institutes of Biomedical Sciences, Fudan University, Shanghai, China, [6]Baylor College of Medicine and Texas Children's Hospital, Houston, TX, [7]Division of Pediatric Hematology and Oncology, Perlmutter Cancer Center, New York University Langone Health, New York, [8]Tumor Cell Biology, St. Jude Children's Research Hospital, Memphis, TN, [9]Oncogenesis and Development Section, National Human Genome Research Institute, National Institutes of Health, Bethesda, MD, USA, [10]Texas Children's Cancer and Hematology Centers, Baylor College of Medicine, Houston, TX, [11]Cancer Science Institute of Singapore, National University of Singapore, Singapore, [12]Department of Medicine, Yong Loo Lin School of Medicine, National University of Singapore, Singapore, [13]Department of Pathology, St. Jude Children's Research Hospital, Memphis, TN, [14]Department of Oncology, St. Jude Children's Research Hospital, Memphis, TN, [15]Hematological Malignancies Program, St. Jude Children's Research Hospital, Memphis, TN, [16]Department of Pediatrics and Center for Childhood Cancer Research, Children's Hospital of Philadelphia and the Perelman School of Medicine at the University of Pennsylvania, Philadelphia, PA, [17]Division of Oncology, Department of Pediatrics, Center for Childhood Cancer Research, Children's Hospital of Philadelphia and Perelman School of Medicine, University of Pennsylvania, Philadelphia, PA, [18]Department of Pediatrics, Benioff Children's Hospital and the Helen Diller Family Comprehensive Cancer Center, University of California San Francisco, San Francisco, CA

Abstract

RUNX1 is a transcription factor critical for definitive hematopoiesis and genetic alterations in *RUNX1* have been implicated in both benign and malignant blood disorders, particularly of the megakaryocyte and myeloid lineages. Somatic *RUNX1* mutations are reported in B- and T-cell acute lymphoblastic leukemia (B-ALL and T-ALL), but germline genetic variation of *RUNX1* in these lymphoid malignancies have not been comprehensively investigated. Sequencing 4,836 children with B-ALL and 1,354 cases of T-ALL, we identified 31 and 18 unique germline *RUNX1* variants in these two ALL subtypes, respectively. *RUNX1* variants in B-ALL were predicted to have minimal impact. By contrast, 54.5% of variants in T-ALL result in complete or partial loss of RUNX1 activity as a transcription activator *in vitro*, with dominant negative effects for 4 variants. Ectopic expression of dominant negative deleterious *RUNX1* variants in human CD34+ cells repressed differentiation into erythroid, megakaryocytes, and T cells, while promoting differentiation towards myeloid cells. We then performed chromatin immunoprecipitation profiling in isogenic T-ALL models with variants introduced by genome editing of endogenous *RUNX1*. We observed highly distinctive patterns of DNA binding and target genomic loci by RUNX1 proteins encoded by the truncating vs missense variants. The p.G365R *RUNX1* variant resulted in a novel methylation site in RUNX1 and alteration in its interaction with CBFβ. Further whole genome sequencing showed that *JAK3* mutation was the most frequent somatic genomic abnormality in T-ALL with germline *RUNX1* variants. Consistently, co-introduction of *RUNX1* variant and *JAK3* mutation in hematopoietic stem and progenitor cells in mouse gave rise to T-ALL with early T-cell precursor phenotype *in vivo*, compared to thymic T-ALL seen in mice with *JAK3* mutation alone. Taken together, these results indicated that *RUNX1* is an important predisposition gene for ALL, especially in T-ALL and also pointed to novel biology of RUNX1-mediated leukemogenesis in the lymphoid lineages.

Introduction

Acute lymphoid leukemia (ALL) is the most common cancer in children. The exact cause of ALL is incompletely understood, although somatic genomic abnormalities are well documented affecting a wide range of signaling pathways. There is also growing evidence of inherited susceptibility to ALL. For example, common genetic polymorphisms in genes such as *IKZF1*(1), *ARID5B* (2), *CDKN2A*(3), *GATA3* (4, 5), *CEBPE*(6), and *PIP4K2A*(7) are associated with the risk of ALL in an age- and subtype-dependent manner. On the other hand, rare germline variants have been linked to familial predisposition to childhood ALL, and collectively about 5% of sporadic ALL cases harbor pathogenic variants in *TP53*(8), *ETV6*(9), and *IKZF1*(1). These findings point to a strong genetic basis of inter-individual variability in ALL risk.

The RUNX1 protein plays key roles in definitive hematopoiesis (10). RUNX1 functions as a transcription factor by forming a heterodimer with core binding factor β (CBFβ). RUNX1 consists of a Runt homology domain (RHD) responsible for DNA binding and cofactor interaction (11) and the C-terminal transcriptional activation domain (TAD) that recruits co-activators and activates the expression of RUNX1 target genes (12). *RUNX1* germline variants are associated with familial platelet disorder (FPD). Many patients with FPD develop leukemia later in life, predominately acute myeloid leukemia (AML) and myelodysplastic syndrome (MDS) (13-16). Somatic *RUNX1* mutations, most of which occur in the RHD and TAD, have been identified in both B- and T-ALL(17). *RUNX1* mutation is related to poor prognosis in T-ALL(17). Although somatic and germline *RUNX1* variants associated with ALL have been reported, their pattern, prevalence, and functional consequences in B-ALL and T-ALL have not been comprehensively investigated.

Here we report results from targeted germline sequencing of 6,190 children with B- or T-ALL enrolled in frontline Children's Oncology Group (COG) and St. Jude Children's Research Hospital (St. Jude) ALL trials. We observed a lineage-specific pattern of germline variation in the *RUNX1* gene, with deleterious variants exclusively present in T-ALL patients. Furthermore, we experimentally characterized *RUNX1* variants for their effects on transcription factor activity,

84 subcellular localization, cofactor interaction, *in vitro* hematopoiesis, and genome wide RUNX1
85 binding profile. Finally, we examined the somatic genomic landscape of T-ALL arising from
86 *RUNX1* germline variants and modeled *RUNX1*-mediated leukemogenesis in mouse models.

Results

Identification of germline *RUNX1* variants in pediatric ALL

To comprehensively characterize inherited *RUNX1* variations in ALL, we performed targeted sequencing in germline DNA of 4,836 patients with newly diagnosed B-ALL and 1,354 patients with T-ALL enrolled on COG and SJCRH frontline trials (**Figure 1A and Table 1**). We identified 31 unique variants in 61 B-ALL cases and 18 unique variants in 26 T-ALL cases. Seven of these variants were found in both B- and T-ALL (**Figure 1A and Table 1**).

Of the 31 variants in B-ALL, 6 were not observed in the general population (Genome Aggregation database, gnomAD, n = 15,496), 18 were rare with a maximum allele frequency of 0.00122%, and the remaining 7 were considered common variants with allele frequency > 0.01% (**Figure 1A and Table 1**). All the variants in B-ALL except one were missense, most of which are in the C-terminus distal to the DNA binding runt-homology domain (RHD, **Figure 1B**). Of the 18 variants in T-ALL cases, 8 were absent in the gnomAD dataset, 5 were rare with a maximum allele frequency of 0.00239%, and the remaining 5 were common variants (**Figure 1A and Table 1**). 27.8% of variants identified in T-ALL were frameshift or nonsense, including p.K117* and p.S141fs which truncated both the RHD and the transcription activation domain (TAD, **Figures 1B and S1**) and p.Q213fs, p.R232fs, and p.Y287* that resulted in the loss of TAD only (**Figure S1**). Seven missense and 1 in-frame deletion variants in T-ALL were distributed across *RUNX1*. This pattern of variant distribution is significantly different from *RUNX1* germline variants in familial platelet disorder with associated myeloid malignancy (**Figure 1C**)(18), in which the majority of missense variants are localized in the DNA-binding domain (RHD).

Effects of *RUNX1* variants on transcriptional regulation, cellular localization, and protein–protein interaction

To understand how germline *RUNX1* variants affect gene function, we first examined their transcription activator activity using the luciferase reporter assay in Hela cells. With *SPI1* as the

RUNX1 target gene (19), none of the germline variants identified in B-ALL showed a significant impact on reporter gene transcription compared to the wildtype protein and therefore were not studied further (**Figure 2A**). Among *RUNX1* alleles seen in T-ALL, all frameshift and nonsense variants (p.K117*, p.S141fs, p.S213fs, p.R232fs, and p.Y287*) and also missense variant G365R caused significant reduction of RUNX1 activity in this assay (**Figure 2B**). To further characterize these *RUNX1* variants in a more relevant cellular context, we engineered the Jurkat T-ALL cell line in which each *RUNX1* variant of interest was individually inserted into the safe harbor AAVS1 locus (**Figure S2**)(20) and a GFP tag was added to the C-terminus of RUNX1 target gene *GZMA(21)* (**Figure 2C and S3**). Using this model system, RUNX1 transactivation activity could be directly measured as the GFP intensity in *RUNX1* variants knock-in cells, in the presence of endogenous *RUNX1* (**Figure 2D**). As shown in **Figure 2E**, the introduction of WT *RUNX1* as well as most missense variants (p.N153Y, p.T246M, p.A329T, p.P359R, and p.M418V) led to robust GFP signals relative to cells with no *RUNX1* insertion at the AAVS locus, confirming wildtype like transcription activator activity. By contrast, cells with K117* and S141fs showed only baseline GFP signals, indicating complete loss of RUNX1 function. Insertion of the p.Q213fs, p.R232fs, p.Y287*, and p.G365R variants resulted in the lowest GFP intensity, suggesting these variants not only lost their transcription activator activity but also repressed endogenous RUNX1 in a plausibly dominant-negative manner.

We next analyzed subcellular localization and CBFβ cofactor interaction of all deleterious variants, including p.K117*, p.S141fs, p.Q213fs, p.R232fs, p.Y287*, and p.G365R (**Figure S1**). Fluorescence microscopy of HEK293T cells ectopically expressing *RUNX1* variants showed that p.K117* and p.S141fs proteins were mis-localized to the cytoplasm, whereas p.Q213fs, p.R232fs, p.Y287*, p.G365R proteins remained in the nucleus (**Figure 2F**). In co-immunoprecipitation assay, p.K117* and p.S141fs variant proteins were no longer associated with CBFβ most likely due to the absence of RHD, whereas all the other variants retained the ability to interact with this co-factor (**Figure 2G**).

Effects of *RUNX1* variants on the differentiation and proliferation of human cord blood CD34+ cells *in vitro*

We next sought to examine the effects of *RUNX1* variants on hematopoietic differentiation *in vitro* using human cord blood CD34+ cell as the model system. Because p.K117* and p.S141fs simply resulted in complete loss of function with no dominant negative effects, we chose not to further characterize them. For the remaining deleterious variants, we selected p.R232fs, p.Y287* and p.G365R to represent frameshift, nonsense, and missense variants, respectively (**Figure S4**). RUNX1 variants were ectopically expressed in human CD34+ cells which were then subjected to differentiation, proliferation, and apoptosis assays *in vitro* (**Figure 3A**).

In colony formation assays conditioned for erythroid and myeloid progenitor cell growth, the expression of p.R232fs, p.Y287*, and p.G365R significantly repressed burst-forming unit erythroid (BFU-E) and increased colony-forming unit granulocyte-macrophage (CFU-GM) colonies compared to CD34+ cells transduced with WT RUNX1 (**Figure 3B**). The immunophenotype of these progenitor cells were also confirmed by flow cytometry (**Figure S5A**). Long-term culture showed that the *RUNX1* variant-transduced CD34+ cells proliferated faster with concomitant reduction in apoptosis, compared to WT *RUNX1* transduced cells (**Figure 3C-D and S5B**).

With culture conditions for megakaryocyte differentiation, expression of RUNX1 variants consistently resulted in a significant reduction of CD41a+/CD42b+ population compared to WT (**Figure 3E**). These RUNX1 variants also significantly repressed the generation of CD5+/CD7+ T cells from the CD34+ population (**Figure 3F**). Collectively, these results suggested that *RUNX1* variants promoted myeloid differentiation while repressing megakaryocyte and T-cell differentiation *in vitro*.

***RUNX1* variants have highly distinctive patterns of DNA binding and are associated with altered post-translational modifications**

To understand the molecular effects of *RUNX1* variants, we comprehensively profiled RUNX1 binding across the genome using chromatin immunoprecipitation-sequencing (ChIP-seq). We first

engineered three isogenic Jurkat cell lines in which each of the three *RUNX1* variants (p.R232fs, p.Y287*, and p.G365R) was individually knocked-in at the endogenous locus in a hemizygous fashion to represent heterozygous genotype seen in patients (**Figure 4A and 4B**). In these models, we introduced the HA tag and TY1 epitope tags at the 3' end of the coding exon on the variant and WT *RUNX1* alleles, respectively (**Figure S6-S10**). This enabled us to separately profile variant or WT RUNX1 binding using HA or TY1 antibodies (**Figure S9C-D and S10C-D**). We also generate two single clones, in which both allele were wildtype *RUNX1*, but tagged with HA and TY1 seperately (**Figure S8 and S10**).

ChIP-seq showed that all three variants have a largely overlapping binding profile as WT RUNX1 in T-ALL genome (**Figure 4C**). However, the C-terminal truncating variants p.R232fs and p.Y287* exhibited a much similar binding pattern compared with missense p.G365R variant and wildtype RUNX1 (**Figure 4D and S11**), as evidenced by the pearson correlation coefficient of ChIP-seq signals. Even though these variant proteins maintained the DNA binding domain, their DNA binding preference was different from wildtype or full-length missense mutation RUNX1.

Interestingly, the p.G365R variant gave rise to a novel methylation site in RUNX1, with mono- or di-methylation of the arginine residue confirmed by mass spectrometry and Western blot analysis (**Figure 4E and 4F**). Immunoprecipitation–mass spectrometry results suggested that RUNX1 protein methylation at this site may disrupt its interaction with TUBB family proteins (TUBB2A, TUBB2B, TUBB4B, TUBB5, TUB8, *et al*.) and heat shock proteins, but with an increase of CBFβ binding (**Table S1**).

Somatic genomic abnormalities in T-ALL with germline *RUNX1* variants

To characterize the somatic genomic landscape of T-ALL with germline *RUNX1* variants, we analyzed whole genome seq of six cases with p.K117*, p.S141fs, p.Q213fs, p.R232fs, p.Y287*, and p.G365R variants, which were contrasted with 263 T-ALL with somatic mutations in *RUNX1* or WT genotype (22). Five of six T-ALL (83.3%) with germline *RUNX1* variants had a somatic *JAK3* mutation, significantly higher compared to the frequency of *JAK3* mutation percentage in T-

ALL cases without germline variants in *RUNX1* (7.6%, p-value = 2.59×10^{-5}) (22) or T-ALL cases with somatic mutations in *RUNX1* (27.3%, p-value = 0.05) (**Figure 5A**). *JAK3* mutations in T-ALL cases with germline *RUNX1* variants were located in either the pseudo-kinase domain (M511I and R657Q) or in the kinase domain (L950V, **Figure S12 and Tables S2 and S3**). Of interest, the patient with a germline *RUNX1*-R232fs variant also subsequently acquired a somatic *RUNX1* mutation (R169_E5splice_region).

We also performed RNA-seq of T-ALL with germline *RUNX1* variants and compared the expression profile with cases with germline *RUNX1* variants, somatic *RUNX1* mutations or WT *RUNX1* (N = 4, 11 and 252, respectively). Based on hierarchical clustering of global expression profile, *RUNX1*-variant cases (either germline or somatic) consistently clustered with T-ALL with early T-cell precursor immunophenotype (ETP) or near-ETP cases (**Figure 5B**). These results are consistent with previous reports of the preponderance of *RUNX1* variants in ETP T-ALL (23).

RUNX1 **and** ***JAK3*** **mutation-induced ETP phenotype in murine bone marrow transplantation model**

To model *RUNX1*-related T-ALL leukemogenesis, especially in conjunction with somatic *JAK3* mutation, we introduced different combinations of *RUNX1* and *JAK3* mutations ($RUNX1^{R232fs}$ and $JAK3^{M511I}$) into mouse hematopoietic progenitor cells ($Lin^-/Sca\text{-}1^+/C\text{-}Kit^+$) and monitored leukemia development *in vivo* after transplantation. We hereafter refer to recipient mice with LSK cells transduced with empty vector, $RUNX1^{R232fs}$, $JAK3^{M511I}$, and $JAK3^{M511I}/RUNX1^{R232fs}$ as "control", "$RUNX1^{M}$", "$JAK3^{M}$", and "$JAK3^{M}RUNX1^{M}$" mice, respectively. At 4 months, peripheral leukocyte counts of $JAK3^{M}$ and $JAK3^{M}RUNX1^{M}$ mice (41.78 ± 44.3 E3 cells/μL and 14.93 ± 3.42 E3 cells/μL respectively) were significantly higher than control mice (8.84 ± 2.00 cells/μL), and the lowest peripheral leukocyte counts were seen in $RUNX1^{M}$ mice (6.10 ± 2.03 cells/μL, **Figure S13A**). Flow cytometry analysis at this time point showed a significant increase of CD8+ T cells in $JAK3^{M}$ mice (**Figure S13B and C**), compared with control mice. By contrast, $JAK3^{M}RUNX1^{M}$ mice showed an

increase in Mac1+ population and lower T cell population, suggesting an outgrowth of cells with ETP immunophenotype (**Figure S13B and C**).

At 6 to 10 months after transplantation, both *JAK3*^{M}*RUNX1*^{M} and *JAK3*^{M} mice developed overt leukemia presented with leukocytosis and splenomegaly, with 66.7% and 100% mice developed leukemia, respectively (**Figure 5C-E and S14**). The thymus of *JAK3*^{M}*RUNX1*^{M} mice showed a significantly increase of CD4-CD8- (DN) T cells, particularly DN1 cells, as compared with *JAK3*^{M} mice (**Figure 5F-G**). Circulating leukemic cells of *JAK3*^{M}*RUNX1*^{M} mice showed a markedly higher Mac1+ population, but lower lymphoid surface marker as compared with *JAK3*^{M} mice (**Figure 5H**). Also, flow analysis of spleen and bone marrow showed a similar leukemia immunophenotype as peripheral blood (**Figure 5H**). These results indicate that *JAK3*^{M}*RUNX1*^{M} induced the ETP-ALL phenotype *in vivo*. There was also a trend for higher Mac1+ cells with lower level of CD3+ cells in the peripheral blood of *RUNX1*^{M} mice but they never developed leukemia within this timeframe (**Figure S13**).

Discussion

RUNX1 plays significant roles in definitive hematopoiesis by regulating the differentiation of myeloid, megakaryocyte, and lymphoid lineages. In this study, we comprehensively investigated *RUNX1* variants in germline ALL samples from patients and identified highly deleterious germline *RUNX1* variants in T-ALL cases, most of which were frameshift or nonsense variations. By multilayer functional experiments and comprehensive epigenomic and genomic profiling analyses, we systematically characterized *RUNX1* variant functions and identified *JAK3* mutations as predominant co-operating somatic lesions in T-ALL. Furthermore, *RUNX1* variant, in conjunction with mutant *JAK3*, directly gave rise to ETP-ALL *in vivo*. These findings advance our understanding of the role of *RUNX1* in the predisposition to childhood ALL.

As a crucial transcription factor that regulates the hematopoietic differentiation of multiple lineages, *RUNX1* is one of the most frequent target genes of chromosomal translocation, mutation, and copy number alteration in different hematopoietic diseases and leukemia. *RUNX1* germline variants are associated with familial platelet disorder with associated myeloid malignancy (FPDMM, OMIM #601399), also known as FPD or FPD/AML (13, 14, 16, 24). Although most patients with FPD progress to myeloid malignancies, ALL has been reported in a minority of cases (14, 15). In MDS and AML with germline *RUNX1* variants, somatic *RUNX1* mutations are the most frequently observed genomic alteration, suggesting they are one of the cooperating events for leukemia progression (18, 25). Other studies identified somatic mutations in *CDC25C*, *GATA2*, *BCOR*, *PHF6*, *JAK2*, *DNMT3A*, *TET*, *ASXL1* albeit with lower frequencies (18, 25, 26). By contrast, we identified *JAK3* mutations as the predominant co-occurring event with *RUNX1* germline variants in T-ALL, which consistently drove an ETP phenotype in patients and in mouse models. Therefore, we postulate that while germline *RUNX1* variants disrupt normal hematopoiesis and generally increase the risk of leukemia, the lineage specification of these hematological malignancies is mostly dictated by secondary mutations acquired later in life.

Activating *JAK3* mutations have been reported in T-ALL (23). *In vivo* studies using a murine bone marrow transplantation model showed that *JAK3* mutations in the pseudo-kinase domain caused T-cell lymphoproliferative disease that progressed to T-ALL, mainly by increasing the CD8+ cell population (27, 28). This is in line with our observation that *JAK3*^{M} mice exhibited a significant accumulation of CD8+ cells in thymus, peripheral blood, spleen, and bone marrow. However, *JAK3*^{M}*RUNX1*^{M} mouse developed lymphoid leukemia with a completely distinctive phenotype which recapitulated human ETP T- ALL features similar to previous reported ETP-ALL mouse models (*e.g.,* circulating leukemic cells expressed the myeloid cell marker Mac1, but not the lymphoid markers CD8/CD3)(29, 30). Also, the CD4-CD8- (DN), especially DN1 population was particularly enriched in thymocytes from *JAK3*^{M}*RUNX1*^{M} mice, as compared with *JAK3*^{M} mice. Alongside genomic findings in T-ALL patients, these *in vivo* experiments indicate that *RUNX1* dominant-negative variants plus *JAK3*-activating mutations most likely result in the ETP T-ALL.

A recent study by Brown et al. comprehensively described the genomic landscape of *RUNX1*-related FPD and myeloid malignancy from 130 families (18). In this cohort, missense and truncating germline *RUNX1* variants were equally represented. While truncating variants occurred in both the RUNT domain and the activation domain, missense variants were largely restricted to the DNA-binding RUNT domain. This pattern is significantly different from that in the lymphoid malignancies as described herein. In T-ALL, deleterious *RUNX1* variants were predominantly nonsense or frameshift and the only missense variant resided in the activation domain. Unfortunately, we do not have family history for children with T-ALL carrying *RUNX1* germline variants, and therefore cannot ascertain the exact penetrance on leukemia or FPD. However, given the profound effects on RUNX1 activity and a range of phenotypes *in vitro* and *in vivo*, these variants are likely to be pathogenic. In fact, the Y287* variant seen in our T-ALL cohort has been previously linked to FPD and functional characterization indicated that this variant causes defective megakaryocyte differentiation in the iPSC model (31). In B-ALL, almost all variants were missense and localized outside of RUNT domain, likely with little effects on RUNX1 activity.

Although these variants showed little effects on RUNX1 transcriptional activity level, some of them were predicted to be damaging variants by polyphen2 and SIFT (Table 1). More comprehensive functional assays might be needed to definitively determine the effects of these variants.

Genome-wide patterns of RUNX1 binding have been investigated extensively using ChIP-seq assays (21, 32, 33), but there is a paucity of studies directly examining target genes of variant RUNX1. When this was attempted in the past, variant RUNX1 was either ectopically expressed in iPSC or cord blood CD34+ cells, raising the possibility of false positives due to artificially high levels of RUNX1(34). This is also hindered by the lack of antibodies that specifically recognize wildtype but not variant RUNX1. To overcome these issues, we engineered Jurkat cells with heterozygous knock-in of *RUNX1* variants (p.R232fs/WT, p.Y287*/WT, and p.G365R/WT) using the CHASE-KI method (35). In this model, we also introduced the HA and TY1 epitope tags at the 3' end of the coding exon on the variant and WT *RUNX1* allele, respectively. Our model recapitulated *RUNX1* variant status in patients with T-ALL and enabled us to profile variant or wildtype RUNX1 binding using different antibodies. Moreover, our ChIP-seq result indicated that the C-terminal truncating variants p.R232fs and p.Y287* variants actually exhibited a distinct binding pattern than the full-length p.G365R variant and wildtype RUNX1.

In summary, we comprehensively described *RUNX1* germline variants in childhood ALL. Using multiple functional assays, we identified highly deleterious germline variants in T-ALL and their biochemical and cellular effects. In addition, we characterized somatic genomic alterations associated with *RUNX1* germline variation in T-ALL, illustrating the interplay between acquired and inherited genetic variants in the context of leukemia pathogenesis.

Methods

Patients

A total of 6,190 ALL cases were included for RUNX1 targeted sequencing: 4,132 children with newly diagnosed B-ALL enrolled on the Children's Oncology Group (COG) AALL0232 (n = 2,224), P9904/5/6 (n = 1,634), and AALL0331 (n = 274) protocols; 704 children with newly diagnosed B-ALL enrolled on the St.Jude Total XIII and XV protocols; 1,231 children with newly diagnosed T-ALL enrolled on the COG AALL0434 protocols (1,231); and 123 children with newly diagnosed T-ALL enrolled on the St.Jude Total XIII and XV protocols (Figure 1A) (36-39). This study was approved by institutional review boards at SJCRH and COG affiliated institutions and informed consent was obtained from parents, guardians, or patients, and assent from patients, as appropriate. Family histories were not available for patients on the COG studies, and thus ALL cases were considered to be sporadic. Germline DNA was extracted from peripheral blood or bone marrow from children with ALL during remission.

For targeted *RUNX1* sequencing in the sporadic ALL cohort, Illumina dual-indexed libraries were created from the germline DNA of 6,190 children with ALL, and pooled in sets of 96 before hybridization with customized Roche NimbleGene SeqCap EZ probes (Roche, Roche NimbleGen, Madison, WI, USA) to capture the *RUNX1* genomic region. Quantitative PCR was used to define the appropriate capture product titer necessary to efficiently populate an Illumina HiSeq 2000 flowcell for paired-end 2x100 bp sequencing. Coverage of at least 20-fold depth was achieved across the targeted RUNX1 locus for 99.2% of samples. Sequence reads in FASTQ format were mapped and aligned using the Burrows-Wheeler Aligner (BWA)(40, 41), and genetic variants were called using the GATK pipeline (version 3.1)(41), as previously described, and annotated using the ANNOVAR program(42) with the annotation databases including RefSeq(43), Polyphen2(44, 45) and SIFT(46). Non-coding, and synonymous coding variants were excluded from further consideration for this study.

Genomic Analysis of Patient Samples

Whole-genome sequencing and RNA sequencing were performed for T-ALL cases with germline RUNX1 variants, whenever available samples were identified. Whole genome seq was done for matched germline and leukemia samples, whereas RNA-seq was done only for leukemia samples. Briefly, DNA was purified using the QIAamp DNA Blood Mini Kit (Qiagen, 51104), and RNA was purified using the RiboPure RNA Purification Kit (Thermo Fisher Scientific, AM1928). DNA (250-1000 ng) and RNA (500-1000 ng) was sent to St. Jude Hartwell center for sequencing.

Details for functional experiments, leukemia modeling in mouse, genomic analyses, and other experiments can be found in supplemental file.

More detailed methods can be found in supplemental files.

References

1. Churchman ML, Qian M, Te Kronnie G, Zhang R, Yang W, Zhang H, et al. Germline Genetic IKZF1 Variation and Predisposition to Childhood Acute Lymphoblastic Leukemia. *Cancer Cell.* 2018;33(5):937-48 e8.
2. Trevino LR, Yang W, French D, Hunger SP, Carroll WL, Devidas M, et al. Germline genomic variants associated with childhood acute lymphoblastic leukemia. *Nat Genet.* 2009;41(9):1001-5.
3. Xu H, Zhang H, Yang W, Yadav R, Morrison AC, Qian M, et al. Inherited coding variants at the CDKN2A locus influence susceptibility to acute lymphoblastic leukaemia in children. *Nat Commun.* 2015;6:7553.
4. Perez-Andreu V, Roberts KG, Harvey RC, Yang W, Cheng C, Pei D, et al. Inherited GATA3 variants are associated with Ph-like childhood acute lymphoblastic leukemia and risk of relapse. *Nat Genet.* 2013;45(12):1494-8.
5. Perez-Andreu V, Roberts KG, Xu H, Smith C, Zhang H, Yang W, et al. A genome-wide association study of susceptibility to acute lymphoblastic leukemia in adolescents and young adults. *Blood.* 2015;125(4):680-6.
6. Papaemmanuil E, Hosking FJ, Vijayakrishnan J, Price A, Olver B, Sheridan E, et al. Loci on 7p12.2, 10q21.2 and 14q11.2 are associated with risk of childhood acute lymphoblastic leukemia. *Nat Genet.* 2009;41(9):1006-10.
7. Migliorini G, Fiege B, Hosking FJ, Ma Y, Kumar R, Sherborne AL, et al. Variation at 10p12.2 and 10p14 influences risk of childhood B-cell acute lymphoblastic leukemia and phenotype. *Blood.* 2013;122(19):3298-307.
8. Qian M, Cao X, Devidas M, Yang W, Cheng C, Dai Y, et al. TP53 Germline Variations Influence the Predisposition and Prognosis of B-Cell Acute Lymphoblastic Leukemia in Children. *J Clin Oncol.* 2018;36(6):591-9.
9. Moriyama T, Metzger ML, Wu G, Nishii R, Qian M, Devidas M, et al. Germline genetic variation in ETV6 and risk of childhood acute lymphoblastic leukaemia: a systematic genetic study. *Lancet Oncol.* 2015;16(16):1659-66.
10. Wang Q, Stacy T, Binder M, Marin-Padilla M, Sharpe AH, and Speck NA. Disruption of the Cbfa2 gene causes necrosis and hemorrhaging in the central nervous system and blocks definitive hematopoiesis. *Proc Natl Acad Sci U S A.* 1996;93(8):3444-9.
11. Huang G, Shigesada K, Ito K, Wee HJ, Yokomizo T, and Ito Y. Dimerization with PEBP2beta protects RUNX1/AML1 from ubiquitin-proteasome-mediated degradation. *EMBO J.* 2001;20(4):723-33.
12. Kanno T, Kanno Y, Chen LF, Ogawa E, Kim WY, and Ito Y. Intrinsic transcriptional activation-inhibition domains of the polyomavirus enhancer binding protein 2/core binding factor alpha subunit revealed in the presence of the beta subunit. *Mol Cell Biol.* 1998;18(5):2444-54.
13. Owen CJ, Toze CL, Koochin A, Forrest DL, Smith CA, Stevens JM, et al. Five new pedigrees with inherited RUNX1 mutations causing familial platelet disorder with propensity to myeloid malignancy. *Blood.* 2008;112(12):4639-45.
14. Preudhomme C, Renneville A, Bourdon V, Philippe N, Roche-Lestienne C, Boissel N, et al. High frequency of RUNX1 biallelic alteration in acute myeloid leukemia secondary to familial platelet disorder. *Blood.* 2009;113(22):5583-7.

15. Nishimoto N, Imai Y, Ueda K, Nakagawa M, Shinohara A, Ichikawa M, et al. T cell acute lymphoblastic leukemia arising from familial platelet disorder. *Int J Hematol.* 2010;92(1):194-7.
16. Song WJ, Sullivan MG, Legare RD, Hutchings S, Tan X, Kufrin D, et al. Haploinsufficiency of CBFA2 causes familial thrombocytopenia with propensity to develop acute myelogenous leukaemia. *Nat Genet.* 1999;23(2):166-75.
17. Grossmann V, Kern W, Harbich S, Alpermann T, Jeromin S, Schnittger S, et al. Prognostic relevance of RUNX1 mutations in T-cell acute lymphoblastic leukemia. *Haematologica.* 2011;96(12):1874-7.
18. Brown AL, Arts P, Carmichael CL, Babic M, Dobbins J, Chong CE, et al. RUNX1-mutated families show phenotype heterogeneity and a somatic mutation profile unique to germline predisposed AML. *Blood Adv.* 2020;4(6):1131-44.
19. Huang G, Zhang P, Hirai H, Elf S, Yan X, Chen Z, et al. PU.1 is a major downstream target of AML1 (RUNX1) in adult mouse hematopoiesis. *Nat Genet.* 2008;40(1):51-60.
20. Matreyek KA, Stephany JJ, and Fowler DM. A platform for functional assessment of large variant libraries in mammalian cells. *Nucleic Acids Res.* 2017;45(11):e102.
21. Sanda T, Lawton LN, Barrasa MI, Fan ZP, Kohlhammer H, Gutierrez A, et al. Core transcriptional regulatory circuit controlled by the TAL1 complex in human T cell acute lymphoblastic leukemia. *Cancer Cell.* 2012;22(2):209-21.
22. Liu Y, Easton J, Shao Y, Maciaszek J, Wang Z, Wilkinson MR, et al. The genomic landscape of pediatric and young adult T-lineage acute lymphoblastic leukemia. *Nat Genet.* 2017;49(8):1211-8.
23. Zhang J, Ding L, Holmfeldt L, Wu G, Heatley SL, Payne-Turner D, et al. The genetic basis of early T-cell precursor acute lymphoblastic leukaemia. *Nature.* 2012;481(7380):157-63.
24. Michaud J, Wu F, Osato M, Cottles GM, Yanagida M, Asou N, et al. In vitro analyses of known and novel RUNX1/AML1 mutations in dominant familial platelet disorder with predisposition to acute myelogenous leukemia: implications for mechanisms of pathogenesis. *Blood.* 2002;99(4):1364-72.
25. Antony-Debre I, Duployez N, Bucci M, Geffroy S, Micol JB, Renneville A, et al. Somatic mutations associated with leukemic progression of familial platelet disorder with predisposition to acute myeloid leukemia. *Leukemia.* 2016;30(4):999-1002.
26. Yoshimi A, Toya T, Kawazu M, Ueno T, Tsukamoto A, Iizuka H, et al. Recurrent CDC25C mutations drive malignant transformation in FPD/AML. *Nat Commun.* 2014;5:4770.
27. Degryse S, de Bock CE, Cox L, Demeyer S, Gielen O, Mentens N, et al. JAK3 mutants transform hematopoietic cells through JAK1 activation, causing T-cell acute lymphoblastic leukemia in a mouse model. *Blood.* 2014;124(20):3092-100.
28. Cornejo MG, Kharas MG, Werneck MB, Le Bras S, Moore SA, Ball B, et al. Constitutive JAK3 activation induces lymphoproliferative syndromes in murine bone marrow transplantation models. *Blood.* 2009;113(12):2746-54.
29. Booth CAG, Barkas N, Neo WH, Boukarabila H, Soilleux EJ, Giotopoulos G, et al. Ezh2 and Runx1 Mutations Collaborate to Initiate Lympho-Myeloid Leukemia in Early Thymic Progenitors. *Cancer Cell.* 2018;33(2):274-91 e8.

30. Wang C, Oshima M, Sato D, Matsui H, Kubota S, Aoyama K, et al. Ezh2 loss propagates hypermethylation at T cell differentiation-regulating genes to promote leukemic transformation. *J Clin Invest.* 2018;128(9):3872-86.
31. Connelly JP, Kwon EM, Gao Y, Trivedi NS, Elkahloun AG, Horwitz MS, et al. Targeted correction of RUNX1 mutation in FPD patient-specific induced pluripotent stem cells rescues megakaryopoietic defects. *Blood.* 2014;124(12):1926-30.
32. Giambra V, Jenkins CR, Wang H, Lam SH, Shevchuk OO, Nemirovsky O, et al. NOTCH1 promotes T cell leukemia-initiating activity by RUNX-mediated regulation of PKC-theta and reactive oxygen species. *Nat Med.* 2012;18(11):1693-8.
33. Wilkinson AC, Ballabio E, Geng H, North P, Tapia M, Kerry J, et al. RUNX1 is a key target in t(4;11) leukemias that contributes to gene activation through an AF4-MLL complex interaction. *Cell Rep.* 2013;3(1):116-27.
34. Gerritsen M, Yi G, Tijchon E, Kuster J, Schuringa JJ, Martens JHA, et al. RUNX1 mutations enhance self-renewal and block granulocytic differentiation in human in vitro models and primary AMLs. *Blood Adv.* 2019;3(3):320-32.
35. Hyle J, Zhang Y, Wright S, Xu B, Shao Y, Easton J, et al. Acute depletion of CTCF directly affects MYC regulation through loss of enhancer-promoter looping. *Nucleic Acids Res.* 2019;47(13):6699-713.
36. Larsen EC, Devidas M, Chen S, Salzer WL, Raetz EA, Loh ML, et al. Dexamethasone and High-Dose Methotrexate Improve Outcome for Children and Young Adults With High-Risk B-Acute Lymphoblastic Leukemia: A Report From Children's Oncology Group Study AALL0232. *J Clin Oncol.* 2016;34(20):2380-8.
37. Bowman WP, Larsen EL, Devidas M, Linda SB, Blach L, Carroll AJ, et al. Augmented therapy improves outcome for pediatric high risk acute lymphocytic leukemia: results of Children's Oncology Group trial P9906. *Pediatr Blood Cancer.* 2011;57(4):569-77.
38. Pui CH, Sandlund JT, Pei D, Campana D, Rivera GK, Ribeiro RC, et al. Improved outcome for children with acute lymphoblastic leukemia: results of Total Therapy Study XIIIB at St Jude Children's Research Hospital. *Blood.* 2004;104(9):2690-6.
39. Pui CH, Relling MV, Sandlund JT, Downing JR, Campana D, and Evans WE. Rationale and design of Total Therapy Study XV for newly diagnosed childhood acute lymphoblastic leukemia. *Ann Hematol.* 2004;83 Suppl 1:S124-6.
40. Li H, and Durbin R. Fast and accurate short read alignment with Burrows-Wheeler transform. *Bioinformatics.* 2009;25(14):1754-60.
41. McKenna A, Hanna M, Banks E, Sivachenko A, Cibulskis K, Kernytsky A, et al. The Genome Analysis Toolkit: a MapReduce framework for analyzing next-generation DNA sequencing data. *Genome Res.* 2010;20(9):1297-303.
42. Wang K, Li M, and Hakonarson H. ANNOVAR: functional annotation of genetic variants from high-throughput sequencing data. *Nucleic Acids Res.* 2010;38(16):e164.
43. Pruitt KD, Brown GR, Hiatt SM, Thibaud-Nissen F, Astashyn A, Ermolaeva O, et al. RefSeq: an update on mammalian reference sequences. *Nucleic Acids Res.* 2014;42(Database issue):D756-63.
44. Adzhubei IA, Schmidt S, Peshkin L, Ramensky VE, Gerasimova A, Bork P, et al. A method and server for predicting damaging missense mutations. *Nat Methods.* 2010;7(4):248-9.
45. Adzhubei I, Jordan DM, and Sunyaev SR. Predicting functional effect of human missense mutations using PolyPhen-2. *Curr Protoc Hum Genet.* 2013;Chapter 7:Unit7 20.

46. Kumar P, Henikoff S, and Ng PC. Predicting the effects of coding non-synonymous variants on protein function using the SIFT algorithm. *Nat Protoc*. 2009;4(7):1073-81.

Figures and figure legends

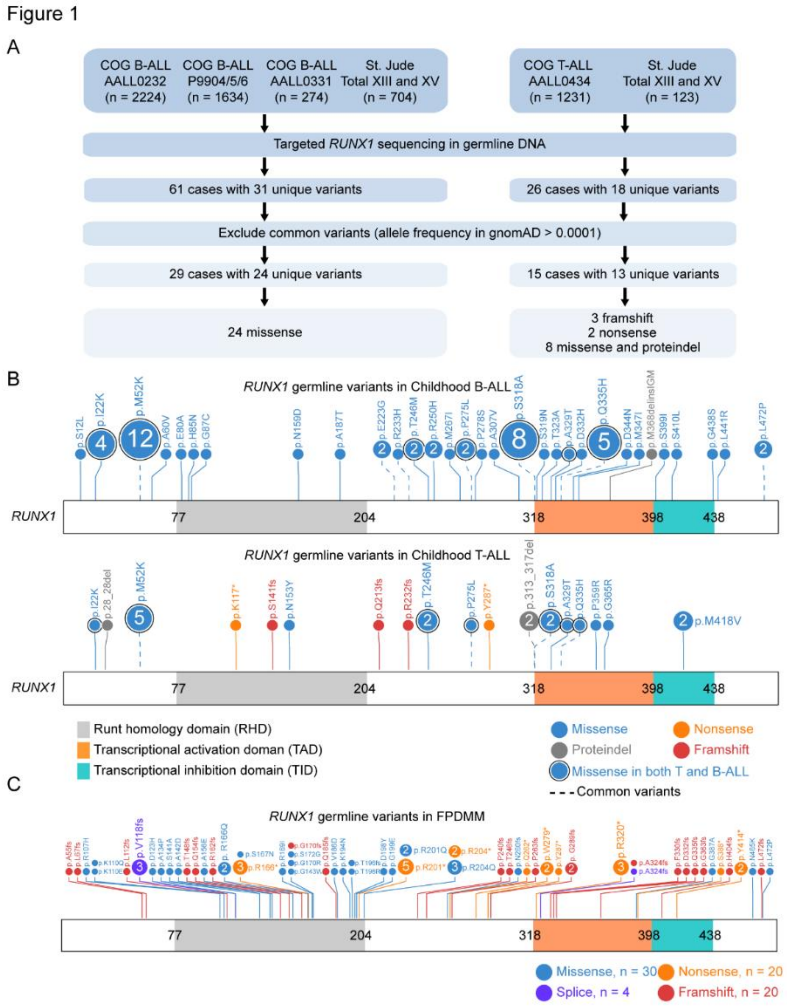

Figure 1. Germline *RUNX1* variants in childhood B- and T-ALL. (A) CONSORT diagram of the Children's Oncology Group (COG) and St. Jude Children's Research Hospital (St. Jude) patients included in this study. (B) Protein domain plot of RUNX1 and the amino acid substitutions predicted to result from the germline *RUNX1* variants identified in this study. The upper panel showed germline *RUNX1* variants in B-ALL cases, and the lower panel showed those in T-ALL cases. (C) Protein domain plot of RUNX1 and the germline RUNX1 variants identified previously in familial platelet disorder with associated myeloid malignancy (FPDMM). Data were retrieved from recently published paper (18).

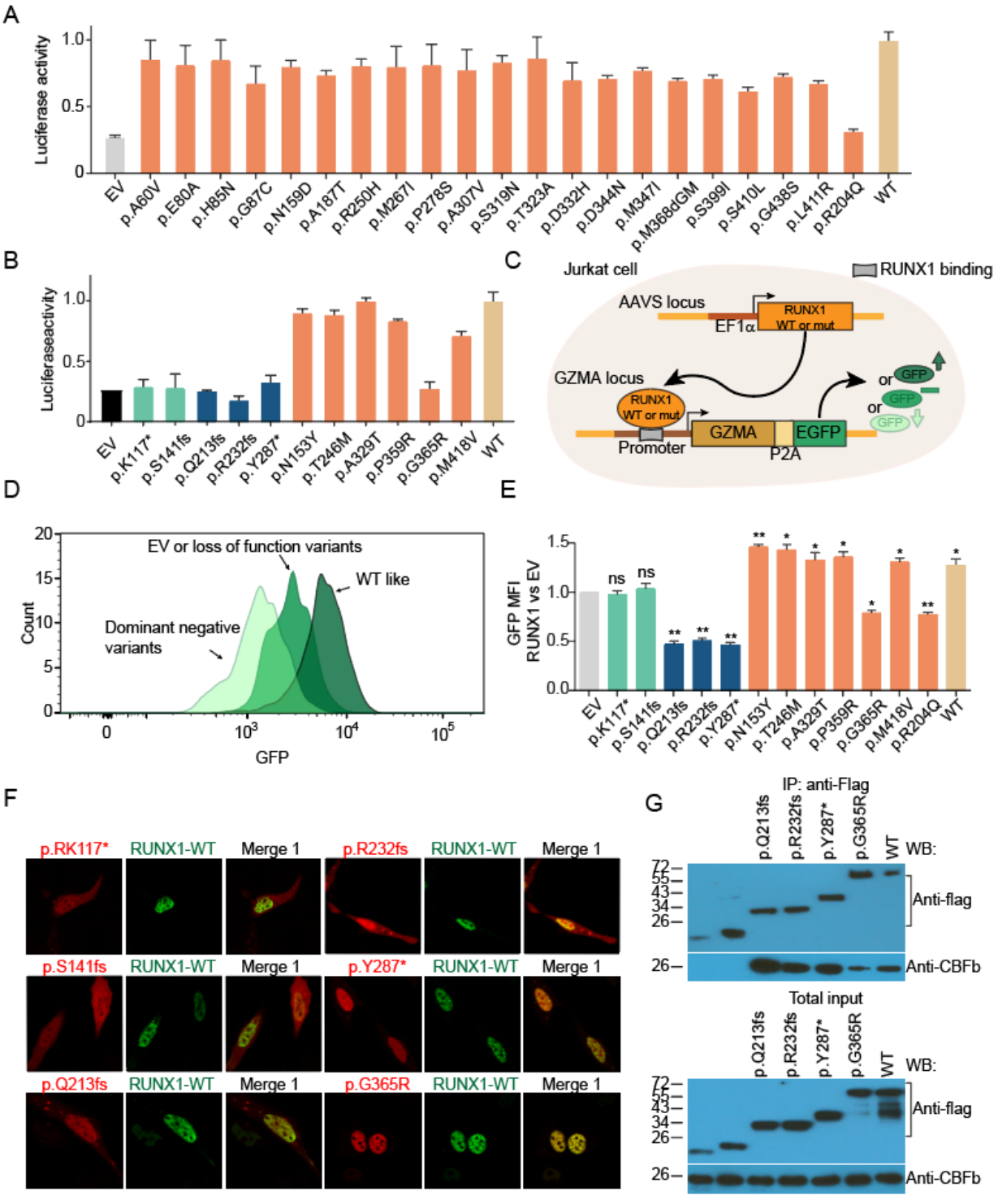

Figure 2. Germline *RUNX1* variants influence transcription factor activity, subcellular localization, and CBFβ interaction. (A) Luciferase reporter gene assay (driven by the *PU.1* promoter in Hela cells) showed minimal effects on transcription factor activity by missense *RUNX1*

variants identified in B-ALL. (B) By contrast, 6 of 11 *RUNX1* variants observed in T-ALL resulted in complete or partial loss of activity, as measured using luciferase reporter gene assay. (C) Design of the Jurkat landing-pad system to measure RUNX1 variant activity in T-ALL. *RUNX1* (either WT or variant) was inserted at the AAVS locus. EGFP coding sequence was knocked at the 3'-end of *GZMA*, a RUNX1 target gene. RUNX1 transcription factor activity was determined by flow cytometry of GFP signal which reflects RUNX1-driven *GZMA* transcription. (D) Flow cytometry analysis of Jurkat cells expressing different *RUNX1* variants. Cells harboring dominant negative, loss of function, and WT like RUNX1 variants exhibited the lowest, moderate, and highest GFP signals, respectively. (E) The GFP signal from Jurkat cells expressing each *RUNX1* variant (relative to empty vector) is shown in bar graph, with error bars indicating standard deviation of triplicates. (F) Immunofluorescence microscopy shows subcellular localization of mCherry-tagged variant proteins and EGFP-tagged WT RUNX1. Variant and WT RUNX1 were fused to mCherry and EGFP and expressed transiently in HEK293T cells, which were then subjected to imaging analyses. (G) Co-immunoprecipitation assay was performed to determine RUNX1-CBFβ interaction for each deleterious variant. Experiments were performed in HEK293T cells. RUNX1 proteins were pulled down using anti-FLAG antibody and the presence or absence of CBFβ in the pellet was examined by immunoblotting.

Figure 3

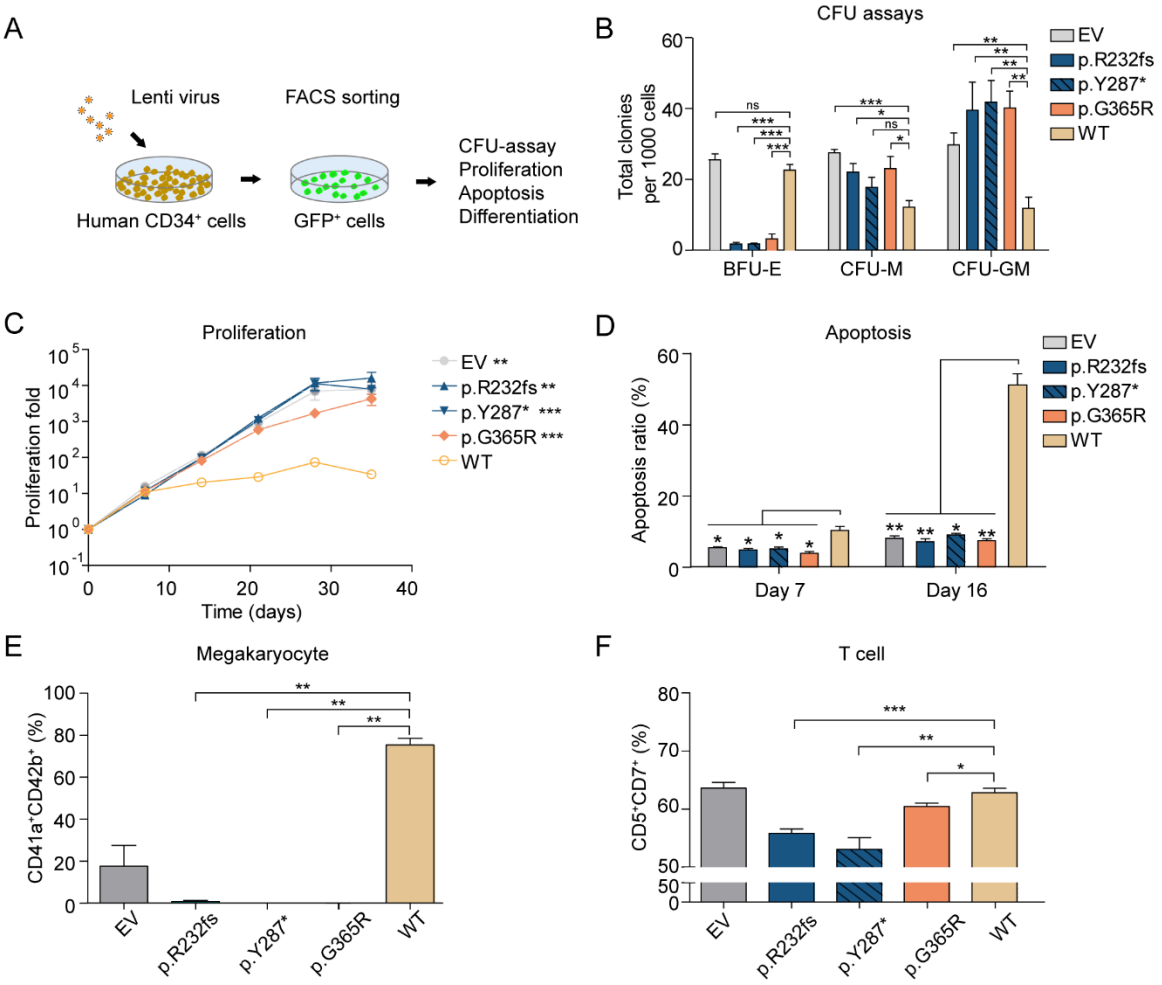

508

509 **Figure 3. *RUNX1* variants affect *in vitro* differentiation of human cord blood CD34+ cells.**
510 (A) The scheme shows the design of in vitro hematopoietic differentiation assay. *RUNX1* variants
511 were lentivirally introduced into human cord blood CD34+ cells. Successfully transduced cells
512 were sorted by flow cytometry and processed for colony forming unit assays, and assessed for
513 cell proliferation and apoptosis, as appropriate. (B) One thousand RUNX1-expressing CD34+
514 cells were plated in MethoCult H4034. The Y-axis shows the count of colonies for each lineage:
515 burst-forming unit erythroid (BFU-E), colony-forming unit-macrophage (CFU-M), and colony-
516 forming unit granulocyte-macrophage (CFU-GM). (C) Proliferation of RUNX1-expressing CD34+
517 cells were monitored for 5 weeks, in Iscove's Modified Dulbecco Medium (IMDM) medium

containing 20% BIT9500, 10 ng/mL FLT-3 ligand, TPO, SCF, IL-3, and IL-6. The number of cells was counted every week for 5 weeks. (D) Apoptosis of RUNX1-transduced CD34+ cells after 7 and 16 days of culture (same culture medium as C) was measured by flow cytometry using Annexin-V and DAPI antibodies. (E-F) CD34+ cells ectopically expressing *RUNX1* variants were also subjected to *in vitro* differentiation assays for megakaryocyte or T cell lineages. Following RUNX1 transduction, cells were cultured in the presence of SFEMII containing megakaryocyte expansion supplement or T-Cell progenitor differentiation supplement for 2 weeks. Megakaryocyte (E) was identified as CD41a+/CD42b+, and T cells (F) were defined as CD5+/CD7+ by flow cytometry.

Figure 4

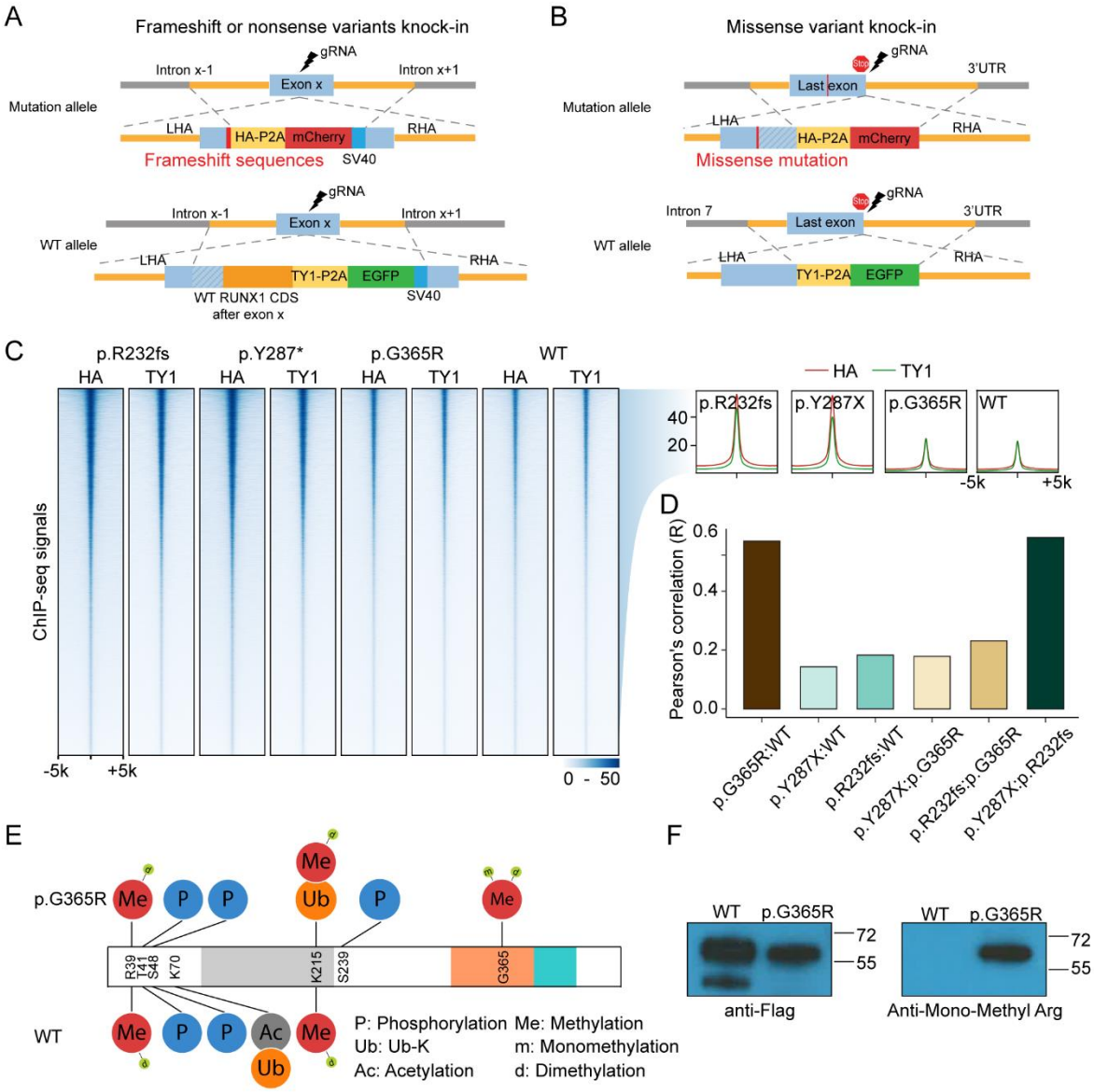

Figure 4. *RUNX1* variants have highly distinctive DNA binding patterns and associated with altered post-translational modifications. (A-B) Schematic representation of engineered Jurkat cell models for RUNX1 binding profiling studies. Variants (p.R232fs, p.Y287*, and p.G365R) were knocked in using CRISPR-cas9 editing at the endogenous locus in a heterozygous fashion. Meanwhile TY1 and HA epitopes were inserted to the coding sequence of WT and variant RUNX1, respectively. This design enables ChIP-seq of each protein simultaneously using two different antibodies. (C) ChIP-seq using HA antibody (recognizing RUNX1 variant) or TY1 antibody (for

535 wildtype RUNX1) showed that activation domain truncating variant RUNX1 (p.R232fs and
536 p.Y287*) recognized largely identical genomic regions as missense variant p.G365R and wildtype
537 RUNX1. Cells with homozygous WT genotype were used as control. (D) Pearson's correlation of
538 WT and variant RUNX1 ChIP-seq signals (HA divided by TY1). (E) Predicted post translational
539 modification of the p.G365R protein showed arginine methylation resulting from the single
540 nucleotide variant. (F) Arginine mono-methylation was confirmed by immunoblotting using an anti-
541 Mono-Methyl Arginine antibody.

Figure 5

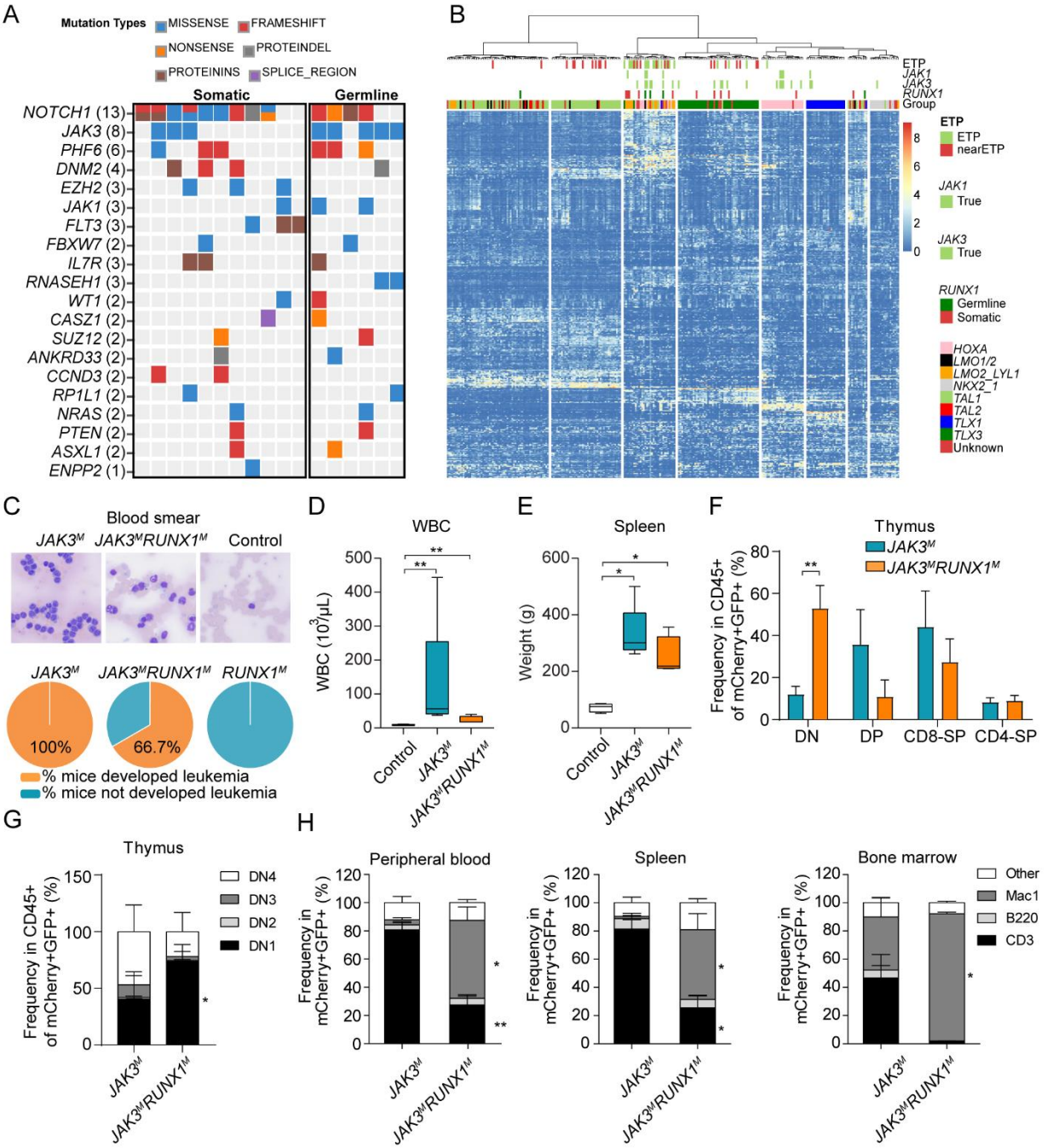

Figure 5. Somatic *JAK3* mutations co-occurs in T-ALL with germline *RUNX1* variants and jointly drive ETP phenotype in mouse models. (A) Somatic *JAK3* mutations were significantly enriched in T-ALL cases with germline *RUNX1* variants. Whole genome seq of remission samples for 17 T-ALL cases, 6 and 11 with germline variants or somatic mutations in *RUNX1*, respectively.

(B) RNA-seq was analyzed for 267 T-ALL cases, including 252, 4, and 11 subjects with WT RUNX1, carrying germline variants or somatic mutations in this gene. Unsupervised clustering shows that RUNX1-variant cases, either germline or somatic, clustered tightly with T-ALL with ETP and near-ETP immunophenotypes. (C) Upper panel: examples of blood smear of *JAK3*^{M} and *JAK3*^{M}*RUNX1*^{M} mice at the time of sacrifice, and control mice after 4 months of transplantation. Lower panel: the percentage of mice developed leukemia in each group. *JAK3*^{M}: 100%, 5 out of 5; *JAK3*^{M}*RUNX1*^{M}: 66.7%, 4 out of 6. (D) Peripheral leukocyte count of *JAK3*^{M}*RUNX1*^{M} (n = 4) and *JAK3*^{M} (n = 5) at the time of sacrifice, and control (n = 7) mice after 4 months of transplantation. (E) Spleen weight of *JAK3*^{M}*RUNX1*^{M} (n = 4), and *JAK3*^{M} (n = 5) mice at the time of sacrifice and control mice (n = 4) after 4 months of transplantation. (F and G) Thymocyte immunophenotype of *JAK3*^{M} and *JAK3*^{M}*RUNX1*^{M} mice at the time of sacrifice. Co-expression of *RUNX1*^{M} and *JAK3*^{M} resulted in a drastic increase in DN1 population compared with mice receiving LSK cells expressing JAK3^{M} only. (H) In peripheral blood, bone marrow, and spleen, *JAK3*^{M}*RUNX1*^{M} mice showed a significant increase in Mac1+ population and a reduction of the CD3+ population compared to *JAK3*^{M} mice.

562 **Table 1. Germline RUNX1 variants in pediatric ALL cases**

Protein (NM_001754)	CHROM	POS	REF	ALT	ExonicFunc.refGene	ALL Subtype (n = case number)	Allele frequence in gnomAD	Polyphen2_HDIV_pred	SIFT_pred
p.L472P	21	36164460	A	G	missense	B-ALL (2)	1.99E-04	Probably damaging	Deleterious
p.L441R	21	36164553	A	C	missense	B-ALL (1)	7.28E-06	Probably damaging	Deleterious
p.G438S	21	36164563	C	T	missense	B-ALL (1)		Probably damaging	Tolerated
p.S410L	21	36164646	G	A	missense	B-ALL (1)	1.56E-05	Probably damaging	Deleterious
p.S399I	21	36164679	C	A	missense	B-ALL (1)	1.74E-05	Probably damaging	Deleterious
p.M368delinsIGM	21	36164771	C	CATGCCC	nonframeshift_insertion	B-ALL (1)	7.34E-05	.	.
p.M347I	21	36164834	C	T	missense	B-ALL (1)	8.79E-06	Benign	Deleterious
p.D344N	21	36164845	C	T	missense	B-ALL (1)	6.20E-05	Probably damaging	Tolerated
p.Q335H	21	36164870	C	A	missense	B-ALL (5) and T-ALL (1)	1.70E-04	Probably damaging	Deleterious
p.D332H	21	36164881	C	G	missense	B-ALL (1)	4.73E-06	Probably damaging	Deleterious
p.A329T	21	36164890	C	T	missense	B-ALL (1) and T-ALL (1)		Possibly damaging	Tolerated
p.T323A	21	36171598	T	C	missense	B-ALL (1)	1.59E-05	Benign	.
p.S319N	21	36171609	C	T	missense	B-ALL (1)		Possibly damaging	Tolerated
p.S318A	21	36171613	A	C	missense	B-ALL (8) and T-ALL (2)	8.13E-04	Possibly damaging	Tolerated
p.A307V	21	36171645	G	A	missense	B-ALL (1)		Possibly damaging	Tolerated
p.P278S	21	36171733	G	A	missense	B-ALL (1)	1.19E-05	Possibly damaging	Tolerated
p.P275L	21	36171741	G	A	missense	B-ALL (2) and T-ALL (1)	2.03E-04	Possibly damaging	Tolerated
p.M267I	21	36206711	C	T	missense	B-ALL (1)	3.93E-05	Benign	Tolerated
p.R250H	21	36206763	C	T	missense	B-ALL (2)	3.91E-05	Probably damaging	Tolerated
p.T246M	21	36206775	G	A	missense	B-ALL (2) and T-ALL (2)	4.61E-05	Probably damaging	Tolerated
p.R233H	21	36206814	C	T	missense	B-ALL (1)	1.67E-04	Probably damaging	Tolerated
p.E223G	21	36206844	T	C	missense	B-ALL (2)	1.24E-04	Probably damaging	Deleterious
p.A187T	21	36231825	C	T	missense	B-ALL (1)	3.98E-06	Probably damaging	Deleterious
p.N159D	21	36252887	T	C	missense	B-ALL (1)		Probably damaging	Deleterious
p.G87C	21	36259232	C	A	missense	B-ALL (1)		Probably damaging	Deleterious
p.H85N	21	36259238	G	T	missense	B-ALL (1)	3.59E-05	Probably damaging	Deleterious
p.E80A	21	36259252	T	G	missense	B-ALL (1)	1.22E-05	Possibly damaging	Deleterious
p.A60V	21	36259312	G	A	missense	B-ALL (1)	7.40E-05	Possibly damaging	Tolerated
p.M52K	21	36259336	A	T	missense	B-ALL (12) and T-ALL (5)	2.46E-04	Probably damaging	Deleterious
p.I22K	21	36265254	A	T	missense	B-ALL (4) and T-ALL (1)	4.01E-06	Benign	Tolerated
p.S12L	21	36421162	G	A	missense	B-ALL (1)	3.98E-06	Benign	Tolerated
p.M418V	21	36164623	T	C	missense	T-ALL (2)		Benign	Deleterious
p.G365R	21	36164782	C	G	missense	T-ALL (1)	9.73E-06	Probably damaging	Deleterious
p.P359R	21	36164799	G	C	missense	T-ALL (1)		Probably damaging	Deleterious
p.313_317del	21	36171614	TTCTGCA	A	nonframeshift_deletion	T-ALL (2)	1.73E-04	.	.
p.Y287X	21	36171704	G	C	stopgain	T-ALL (1)		.	Tolerated
p.R232fs	21	36206815	GC	G	frameshift_deletion	T-ALL (1)		.	.
p.Q213fs	21	36206874	TG	T	frameshift_deletion	T-ALL (1)		.	.
p.N153Y	21	36252905	T	A	missense	T-ALL (1)		Probably damaging	Deleterious
p.S141fs	21	36252939	C	CGGTT	frameshift_insertion	T-ALL (1)	2.39E-05	.	.
p.K117X	21	36259142	T	A	stopgain	T-ALL (1)		.	Tolerated
p.28_28del	21	36265234	TAGA	T	nonframeshift_deletion	T-ALL (1)	4.62E-05	.	.

563

564 Polyphen2, Polymorphism Phenotyping v2; SIFT, Sorting Intolerant From Tolerant.